A Comparative Scanning Tunneling Microscopy Study of Physisorbed Linear Quadrupolar Molecules: C2N2 and CS2 on Au{111} at 4 K†

ARTICLE *in* THE JOURNAL OF PHYSICAL CHEMISTRY A · MAY 2003

Impact Factor: 2.69 · DOI: 10.1021/jp0226432

4 AUTHORS:

Patrick Han
Tohoku University
25 PUBLICATIONS **593** CITATIONS
SEE PROFILE

Charles Sykes
Tufts University
113 PUBLICATIONS **1,708** CITATIONS
SEE PROFILE

Thomas P. Pearl
North Carolina State University
42 PUBLICATIONS **298** CITATIONS
SEE PROFILE

Paul S Weiss
University of California, Los Angeles
394 PUBLICATIONS **11,864** CITATIONS
SEE PROFILE

A Comparative Scanning Tunneling Microscopy Study of Physisorbed Linear Quadrupolar Molecules: C_2N_2 and CS_2 on Au{111} at 4 K†

P. Han, E. C. H. Sykes, T. P. Pearl, and P. S. Weiss*

Departments of Chemistry and Physics, The Pennsylvania State University, University Park, Pennsylvania 16802-6300

Received: December 21, 2002; In Final Form: April 7, 2003

Submonolayer and near-monolayer coverages of cyanogen (C_2N_2) and carbon disulfide (CS_2) were independently dosed and studied on Au{111} at 4 K. Low-temperature scanning tunneling microscopy was used to investigate the intermolecular and substrate−adsorbate interactions of each of the two chemical species. Both molecules were found to be weakly physisorbed and to form incommensurate structures with respect to the Au{111} lattice. The superlattice formed by the Au{111} reconstruction was determined to have a pronounced effect on the aggregation of the adsorbates. C_2N_2 with a high quadrupole moment does not form an ordered structure and is easily moved by the scanning tunneling microscope tip at 4 K. In contrast, CS_2, having a smaller quadrupole moment, forms a molecular herringbone lattice structure. The Au{111} reconstruction also influences the direction of the CS_2 ordered domains, aligning the CS_2 molecular herringbone lattice unit cell in a 3-fold symmetry. These observations are discussed in terms of the current understanding of the dynamics of 2D solid/liquid−gas interfaces.

Introduction

Understanding intermolecular interactions between adsorbed species on surfaces is fundamental to controlling many useful systems ranging from catalytic processes to the bottom-up design of nanostructures. Over the past few decades, the study of the behavior of small linear molecules adsorbed on flat surfaces such as the graphite basal plane has been a fruitful approach for the purpose of understanding the link between the structure of adsorbed monolayers and their thermodynamic properties.[1] Several studies have focused on systems involving two-dimensional (2D) phases of small linear quadrupolar molecules, such as O_2 and CO_2, adsorbed on graphite to investigate the relationship between the adsorbate−substrate registry and their respective 2D phases and phase transitions.[2−7] However, most of these studies were based on surface averaged diffraction measurements and computer simulations for structural characterization and determination of surface dynamics.

Complementary to the work done on graphite, recent ultrahigh vacuum (UHV) scanning tunneling microscopy (STM) measurements have demonstrated the coexistence of 2D solid/fluid phases on a variety of substrate/adsorbate systems.[8−11] Stranick et al. imaged a 2D solid/gas interface of benzene on Cu{111} at 77 K.[8] In this system, two rows of benzene molecules aligned with both the top and the bottom of the Cu{111} atomic step edges were imaged and assigned to be the 2D solid phase. A third row of benzene molecules at the edge of the 2D solid phase on the upper terrace was also imaged. However, these benzene molecules were imaged with a higher level of streakiness, evidence of transient occupation of these adsorption sites. Stranick et al. concluded that the 2D solid phase is in equilibrium with a 2D gas phase located at the terraces of Cu{111}.

Trost et al. have shown that at 300 K, coadsorbed Cs and O atoms on Ru{0001} exist in both a $(\sqrt{7} \times \sqrt{7})$ 2D quasi-ionic solid phase and a disordered fluid phase.[9] In this system, the fluid phase was imaged by STM as streaky areas that showed the occasional presence of stable clusters with periodic structures. A combination of this latter observation together with LEED measurements at different temperatures indicated a high capacity of the fluid phase to accommodate considerable variations in density. The authors therefore concluded that the Cs/O fluid phase behaves more as a 2D gas than as a 2D liquid. STM was also used by Berner et al. to image a 2D solid/gas equilibrium of sub-phthalocyanine (SubPc) adsorbed on Au{111} at 300 K with molecular resolution.[10] In this system, the 2D honeycomb solid phase formed by SubPc could be imaged together with a streaky disordered fluid phase. A close study of the line scans over both phases showed that the height profile of gaseous SubPc was almost indistinguishable from the profile of SubPc molecules in the solid phase. The observation that within a single line scan single SubPc molecules could be discerned in both phases allowed Berner et al. to propose that the motion of the gaseous SubPc was not induced by the STM tip. The authors were able to use the STM data to estimate the magnitude of the diffusion barrier as well as the condensation energy for 2D island formation.

Time-resolved STM imaging has also been used to probe 2D solid/fluid systems. Yanagi et al. studied the 2D island formation of Pt-tetra-(3,5-di-*tert*-butylphenyl)porphyrin (Pt-TBPP) adsorbed on Cu{100} at 80 K, and were able to image the $(\sqrt{58} \times \sqrt{58})$ structures of individual islands.[11] Here again, the presence of a gas-phase Pt-TBPP was evidenced by the presence of noisy streaks when the tip was scanned over areas away from the ordered islands. Upon sequential imaging of a chosen Pt-TBPP 2D solid island, Yanagi et al. observed that most of the molecules joining or leaving the island did so at the corners of the rectangular island referred to as "kink sites", while the "singular sites" at straight edges of islands showed little activity. This was attributed to the dominant intermolecular interaction of Pt-TBPP molecules, which would favor the addition of

† Part of the special issue "A. C. Albrecht Memorial Issue".

* Corresponding Author. Fax +1-814-863-5516. E-mail: stm@psu.edu.

10.1021/jp0226432 CCC: $25.00
Published on Web 05/20/2003

molecules into the kink sites, resulting in the formation of islands with rectangular contours.

Here we present a comparative study using a low-temperature UHV STM to investigate two systems, namely cyanogen (C_2N_2) and carbon disulfide (CS_2) adsorbed on Au{111} at 4 K. Both molecules are known to play key roles with regard to industrial processes. The study of gold−cyanide interactions is central toward understanding the mechanism of gold extraction and electrodeposition,[12−14] and CS_2 is often used as a model poison in studies of the catalytic reactions involved in hydrodesulfurization.[15−17] The packing structures for both molecules on graphite had been previously assigned on the basis of X-ray diffraction, neutron diffraction, and computer modeling.[7,18] On graphite, ordering is dominated by the intermolecular quadrupolar interaction (quadrupole values: 19.3×10^{-40} C m^2 for C_2N_2 and 11.5×10^{-40} C m^2 for CS_2), with both molecules forming incommensurate herringbone lattices (not to be confused with the herringbone reconstruction of the Au{111} substrate).[19,20] The lack of registry between the adsorbed molecules and the graphite was also attributed to the much larger size of the molecules relative to CO_2, which does form a commensurate herringbone lattice on graphite.[1,5]

The use of STM has allowed us to observe directly the intermolecular and substrate−adsorbate interactions of the two linear quadrupolar molecules, both on a local molecule−molecule scale and also the long-range effect caused by the morphology of the underlying Au{111}. Contrary to intuition, the more quadrupolar C_2N_2 is observed to form a disordered single layer that can be easily manipulated by the STM tip, whereas CS_2 forms herringbone structures as previously predicted on graphite.[7]

Experimental Section

The experiments were performed in UHV at 4 K. All images were scanned in constant-current mode using a home-built low-temperature STM and a cut Pt/Ir tip. The STM has been described in detail elsewhere.[21] An ordered Au{111} surface was obtained through repeated sputter and anneal cycles (1 keV Ar^+ sputtering at ~800 K, annealing at ~800 K). C_2N_2 was produced by the thermal decomposition of solid AgCN.[22] The molecule was dosed via a leak valve and its purity was estimated to be 95% in situ by mass spectrometry. CS_2 was purified by vacuum sublimation prior to use and was introduced into the UHV chamber via a leak valve. The purity of CS_2 was verified in situ and was measured by mass spectrometry to be 98% pure. Both C_2N_2 and CS_2 were deposited on a Au{111} substrate at 4 K by back-filling the UHV chamber. C_2N_2 was studied at 0.6 ML coverage, while CS_2 was studied at two coverages, 0.2 and 0.9 ML. The coverages were determined from the STM images. All tunneling bias voltages are reported with respect to the sample. All images are presented without filtering.

Results and Discussion

Clean Au{111} Substrate. A typical image of the clean Au{111} surface at 4 K before deposition of adsorbates is shown in Figure 1. The $(22 \times \sqrt{3})$ reconstruction is observed as pairs of periodically bent lines of corrugation across terraces and atomic step edges. These lines correspond to the transitional regions where the topmost layer of gold atoms is partially dislocated with respect to both fcc and hcp hollow sites of the bulk layers.[23] The wider depressions between the pairs of soliton walls are regions where the topmost layer of gold atoms is stacked on top of the bulk fcc hollow sites. Surface gold atoms at the narrow depressions are stacked on top of the hcp bulk hollow sites. The 120° bend of the soliton wall pairs delimits the boundaries between rotational domains of the $(22 \times \sqrt{3})$ reconstruction, and therefore two of three possible rotational domains can be observed in Figure 1. Terraces that are 300 Å wide can be commonly found, and single atom defects were observed in concentrations of less than 1 per 1000 surface atoms. Standing waves of the surface state electrons associated with the single atom defects and atomic steps were routinely observed, as seen in the inset of Figure 1. Both C_2N_2 and CS_2 were dosed onto pre-scanned Au{111} surfaces at 4 K under similar conditions.

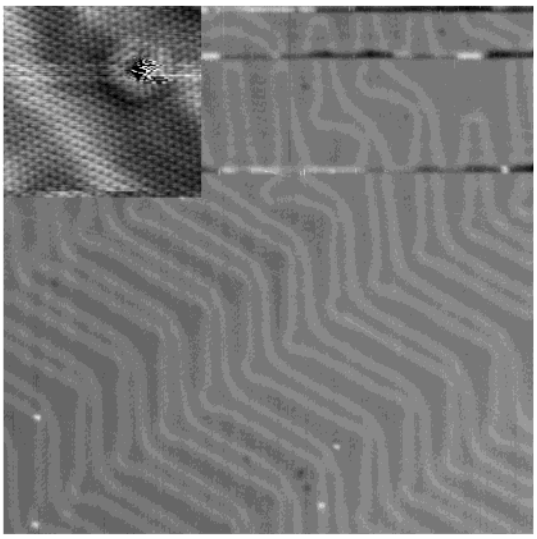

Figure 1. STM image of the clean Au{111} surface (720 Å × 720 Å), recorded at 100 mV sample bias and 100 pA tunneling current, displayed in the derivative mode along the fast scan direction. The inset is a 77 Å × 77 Å topographic image showing an atomically resolved point defect (20 mV sample bias, 800 pA tunneling current).

Adsorption of C_2N_2 on Au{111}. At 0.6 ML coverage, C_2N_2 adsorbs on Au{111} as a disordered single layer as shown in Figure 2A. Individual C_2N_2 molecules appear as oval protrusions. In these images, patches of bare gold area can be discerned. The noisy streaks in the scanning direction of the image show that the tunnel junction over the bare gold patches is far less stable than over the C_2N_2 single-layer. The line scans in these regions are noisy, with the amplitude of the noise in agreement with the apparent height of the molecules. This behavior has been observed previously in other systems and is assigned as a 2D gas phase of the adsorbed molecules.[8,10,24] The line scan shows the average topographic height of the single-layer islands to be 1.4 Å (Figure 2B). The presence of the streaks is dependent of the tunneling conditions during the imaging process. Although the amount of streaking varies from image to image, the tunneling junction is more stable when scanning is performed at a greater tip−sample distance. This fact is confirmed by the image in Figure 3, recorded at 100 mV and 100 pA. Under these tunneling conditions, the tip is close enough that it sweeps away C_2N_2 molecules, revealing the underlying herringbone reconstruction of the gold substrate.

The presence of the herringbone reconstruction is an indication that the substrate−adsorbate interaction is weak, in contrast to other systems such as alkanethiolate monolayers adsorbed on Au{111}, where the strong interaction between sulfur and gold atoms causes Au abstraction resulting in the lifting of the substrate reconstruction.[25] The location of neighboring C_2N_2 molecules with respect to each other can change easily, as shown in Figure 4 which illustrates single molecule evaporation/condensation. The broken-lined circles in Figure 4A denote

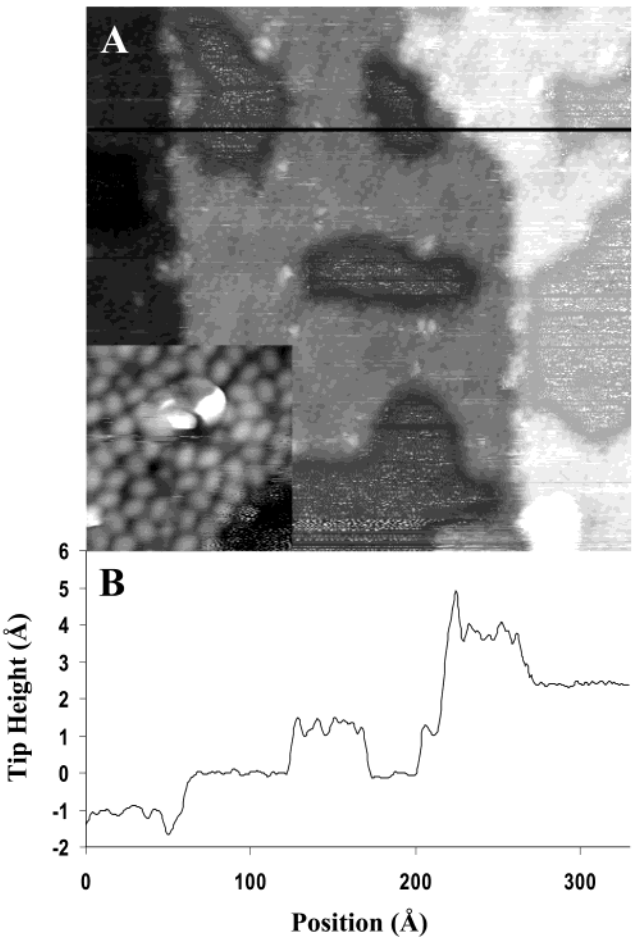

Figure 2. (A) STM image (330 Å × 330 Å) of 0.6 ML of C_2N_2 on Au{111}. This area shows two atomic step edges and the darker fuzzy areas on each terrace are areas of bare gold. The inset is a 44 Å × 44 Å STM image of the disordered C_2N_2 single layer (−700 mV sample bias, 40 pA tunneling current). The gray line in (A) shows the location of the tip−sample separation trace (B), which shows the average apparent topographic height of the C_2N_2 single layer to be 1.4 Å.

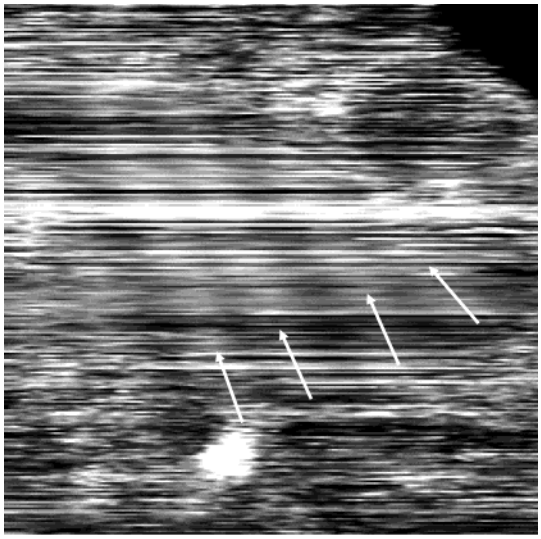

Figure 3. STM image (220 Å × 220 Å) of C_2N_2 dosed on Au{111} at a sample bias of 100 mV and a tunneling current of 100 pA. The tunneling condition set the tip−sample distance to be small so that C_2N_2 molecules were swept away. The white arrows show the location of the soliton walls of the Au{111} reconstruction.

the location of individual molecules in the image. The same circles are displayed in Figure 4B to highlight any translational

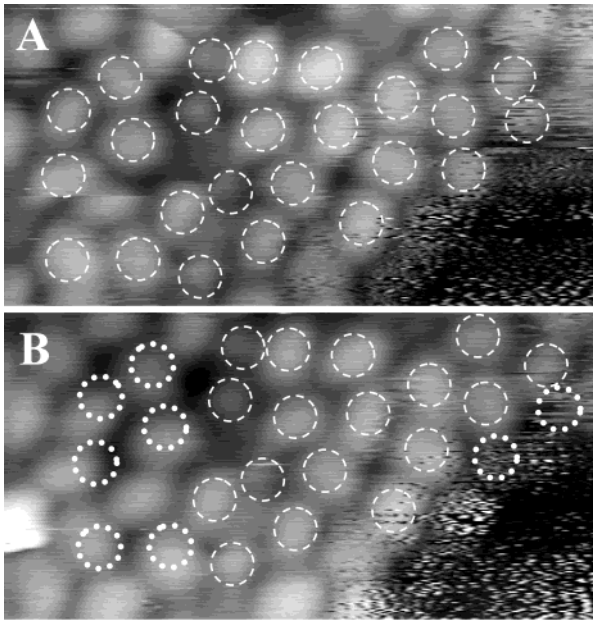

Figure 4. (A) Consecutive high-resolution STM images (44 Å × 22 Å, 400 mV sample bias, 40 pA tunneling current) over the edge of a C_2N_2 single layer. The white broken-lined circles in both images show the position of individual molecules. The dotted circles in (B) display molecules that have changed position between the two images. Two molecules at the edge of the single layer have disappeared.

motion of any molecule between the two images. Dotted-lined circles in Figure 4B denote the molecules that underwent a measurable location change. It is clear from Figure 4 that the molecular positions of individual C_2N_2 molecules are not fixed between each STM image. C_2N_2 molecules located within the single layer undergo tip-induced translational motion. The molecules located at the edge of the single layer can be easily swept away altogether. This suggests that the C_2N_2 single-layer images as a 2D liquid rather than a solid. When a bare gold region surrounded by a 2D C_2N_2 single-layer is repeatedly scanned, the shape and size of the region changes greatly over time. The image sequence in Figure 5 shows the shape of the bare gold perimeter being elongated over time in the scan direction of the image. From these observations, we conclude that C_2N_2 is very weakly physisorbed on Au{111}, where both 2D solid and 2D gas phases coexist. The scanning probe tip affects the 2D solid single layer so much that repeated scanning over the same area melts the solid phase.

Adsorption of CS_2 on Au{111}. At 4 K on Au{111}, CS_2 behaves very differently from C_2N_2. At 0.2 ML coverage, CS_2 molecules form highly ordered single-layer islands (Figure 6A). The packing order is shown in the inset of Figure 6A. The molecules organize in a herringbone arrangement with a unit cell measured to be 8.1 Å × 6.0 Å. This arrangement is attributed to the quadrupolar interactions between the CS_2 molecules where the more negatively charged extremities of the linear molecule are attracted to the more positively charged center.[7,18] This structure is found to be incommensurate with the Au{111} lattice, and the apparent topographic height of the CS_2 islands is 1.5 Å (Figure 6B). It should be noted that the bottom of each of the gold step edges is decorated with a single row of CS_2 molecules. This arises from the interaction between the electrophilic carbon atom of the CS_2 molecule with the higher density of the filled LDOS at the bottom of the atomic step edges.[8,24,26,27] The decorated step edges, combined with island formation, indicate that adsorbate motion must have occurred during deposition.

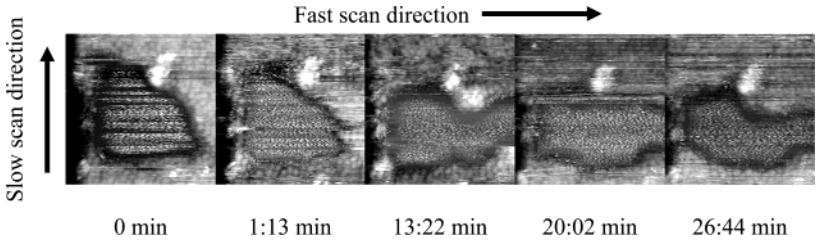

Figure 5. Time-resolved sequence of 110 Å × 110 Å images showing the change in shape and size of an area of bare gold (700 mV sample bias, 20 pA tunneling current). Time is shown in minutes and marks the start of the scan of each respective image.

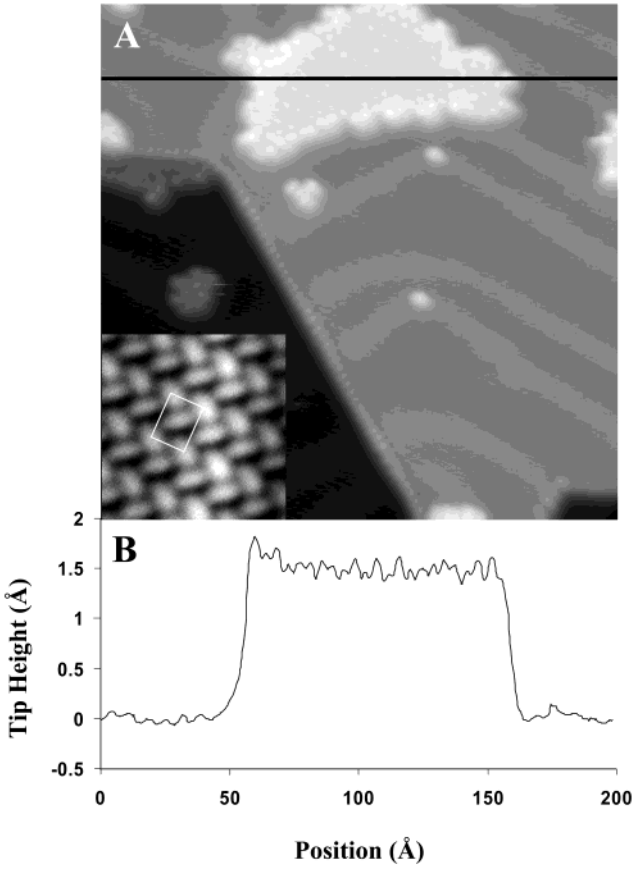

Figure 6. (A) STM image (220 Å × 220 Å) of CS_2 dosed on Au{111} at 0.2 ML coverage (500 mV sample bias, 20 pA tunneling current). Small clusters and islands of CS_2 molecules can be discerned. Single rows of CS_2 molecules along the gold atomic step edge can be observed. The inset shows a 33 Å × 33 Å high-resolution image of the herringbone lattice of a CS_2 single layer island. The white rectangle represents the unit cell of the herringbone lattice (8.1 Å × 6.0 Å). The gray line in (A) shows the location of the tip−sample separation plot as displayed in (B). The average topographic height of the CS_2 island is 1.5 Å.

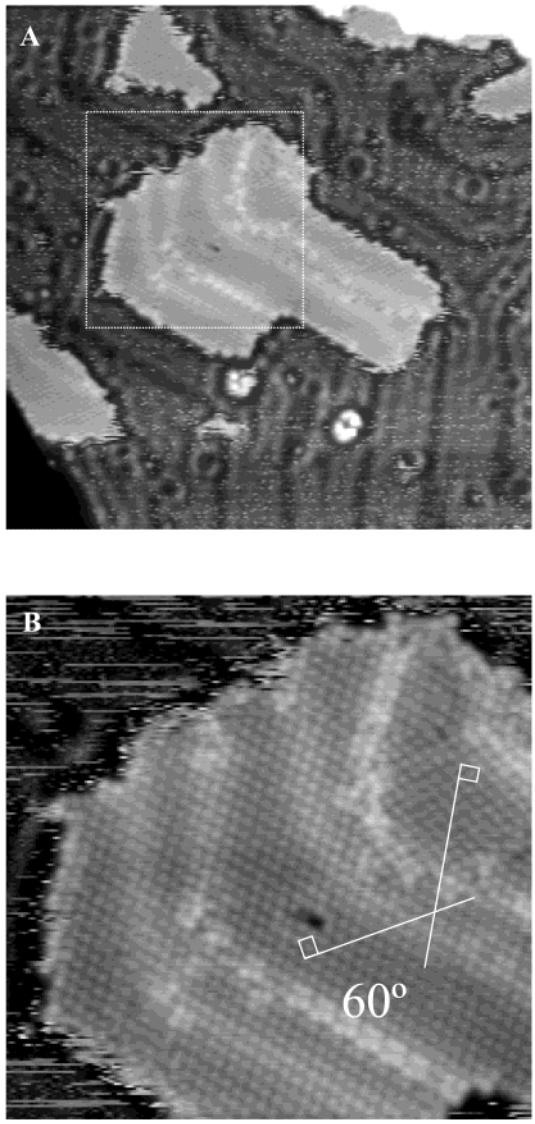

Figure 7. (A) STM image (450 Å × 450 Å) of CS_2 islands dosed on Au{111} at 0.2 ML coverage. The central island of the image shows the alignment of its contour with the soliton walls (500 mV sample bias, 20 pA tunneling current). (B) STM image (184 Å × 184 Å) zoomed in on the aforementioned island. Both rotational and translational domain boundaries can be discerned. The small white rectangles represent the unit cell of rotational domains. The white lines are extensions of those unit cells. The angle between the two rotational domains is measured to be 60°.

At both 0.2 and 0.9 ML coverages, the $(22 \times \sqrt{3})$ reconstruction of the Au{111} is present as shown in Figures 7 and 8. In fact, the presence of the substrate reconstruction affects the island formation of the adsorbate molecules. In Figure 7A, part of the contour of the island at the center of the image is clearly aligned with the underlying Au{111}-$(22 \times \sqrt{3})$ reconstruction. A higher resolution scan over the same island, reveals the presence of several domains of single-layer CS_2 molecules (Figure 7B). Two types of domain boundaries can be discerned, namely translational and rotational boundaries. The packing order of every domain is the same as in the inset of Figure 6A. All CS_2 overlayers imaged had domains with the unit cell direction rotated by 60° (within the ±3° accuracy of our measurements) with respect to each other. This demonstrates that the 3-fold symmetry of the herringbone reconstruction of Au{111} has a long-range effect on the ordering of the CS_2 overlayers.

Figure 8B shows this effect in that two separate domains on different terraces aligned in the same rotational phase, indicating that the aggregation of the molecule is directed by the substrate. It should be noted that, in this same image, small disordered

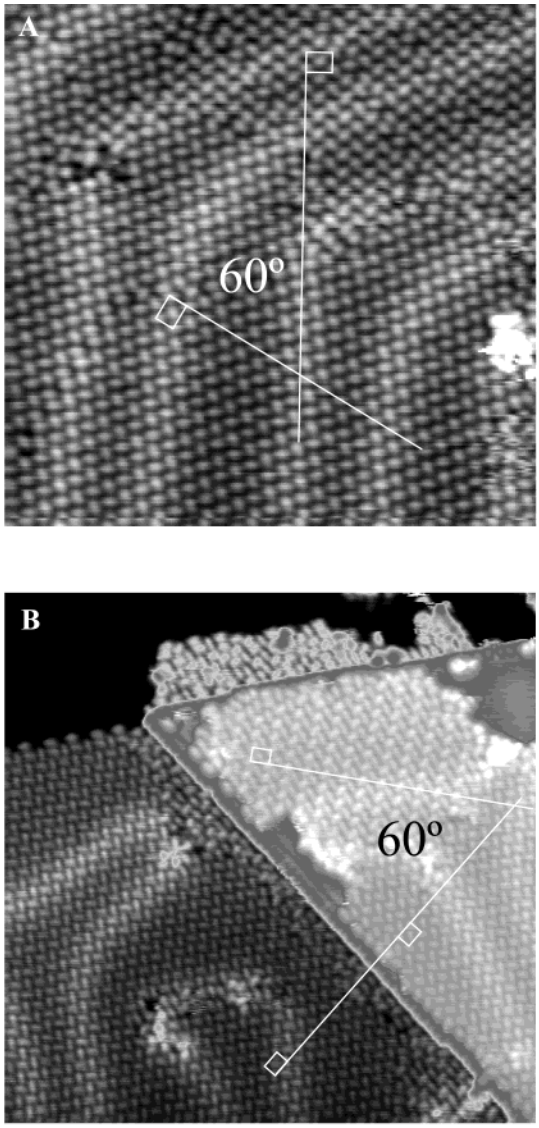

Figure 8. Two STM images showing 0.9 ML coverage CS_2 adsorbed on Au{111}. (A) 170 Å × 170 Å image showing both rotational and translational domain boundaries (500 mV sample bias, 150 pA tunneling current). The two rotational domains are again rotated at 60° with respect to each other. (B) 220 Å × 220 Å image showing a 60° rotation between two domains on the top terrace (−1000 mV sample bias, 50 pA tunneling current). The direction of the one of the domains on the top terrace is shown to be in phase with the domain on the lower terrace.

areas of CS_2 molecules at the lower terrace near the step edge as well as at the U connection of the $(22 \times \sqrt{3})$ gold reconstruction are observed. We attribute this to the confinement effect caused by the near-monolayer coverage. The observed island contour confinement together with the 3-fold symmetry of the CS_2 domains with respect to each other suggests that the substrate has a long-range effect on the direction of the adsorbate domains. This is further confirmed by Figure 9, where the 3-fold symmetry of the rotational phases extends to molecules of different islands located both near a step edge and in the middle of the same terrace.

We propose that the direction of the CS_2 domain is determined during the initial stage of the dosing, when the first molecules become truly physisorbed to the substrate, as subsequent molecules align themselves with the initial physisorbed molecules through transient mobility upon adsorption.[28] Although the actual Au{111} lattice is not directly involved, the $(22 \times \sqrt{3})$ reconstruction acts as a template for the

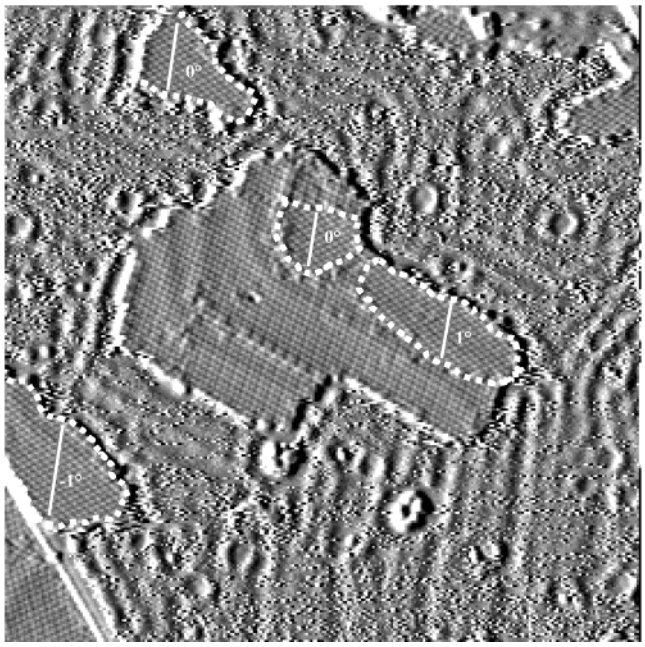

Figure 9. STM image (454 Å × 454 Å) showing different islands of CS_2 molecules on the same terrace. The broken lines delimit domains of the same rotational phase (500 mV sample bias, 20 pA tunneling current, displayed in derivative mode along the fast scan direction). These domains appear slightly offset, by 1°, which is within the margin of error of the measurement. The white solid lines are aligned with the short side of the herringbone lattice unit cell.

aggregation of CS_2, both in influencing the direction of the initial adsorbate surface diffusion and imposing on the substrate domains the same 3-fold symmetry. The rare occurrence of misalignment is attributed to the presence of defects on the substrate and strongly suggests that the forces involved in the process are weak.

Conclusions

When comparing C_2N_2 and CS_2 adsorption on Au{111}, care should be taken over extrapolating previous results concerning overlayer structure of the same molecules on graphite(0001).[7,18] Unlike Au{111}, the graphite basal plane is usually free of reconstruction and molecular ordering can be understood simply in terms of intermolecular quadrupolar interactions directing assembly of the molecular herringbone structure (Figure 6A inset). Our observations of molecular ordering on Au{111} indicate that, even at 4 K, molecules are weakly bound to the surface and 2D growth occurs with a solid/liquid−gas equilibrium. We compare the CS_2 and C_2N_2 overlayer structures, and with molecularly resolved STM images discover that CS_2 forms ordered domains while C_2N_2 images as a disordered 2D solid single layer that is easily melted with the actions of the STM tip. We note that the degree of molecular ordering cannot be predetermined merely by the knowledge of the respective molecule's quadrupolar moment (quadrupole values: 19.3×10^{-40} C m^2 for C_2N_2 and 11.5×10^{-40} C m^2 for CS_2). Instead, the delicate interplay between molecule/molecule and molecule/substrate interactions determines the growth of ordered or amorphous 2D domains in equilibrium with a 2D gas phase. The growth of CS_2 indicates a long-range effect of the Au{111}-$(22 \times \sqrt{3})$ surface on the aggregation of adsorbed organic molecules, and may be useful in future design of building-block molecules and perhaps substrate design, where weaker substrate/molecule interactions are preferred.[29]

Acknowledgment. The authors gratefully acknowledge financial support of the National Science Foundation and the Office of Naval Research. We also thank Sanjini Nanayakkara and Brent Mantooth for their experimental assistance.

References and Notes

(1) Steele, W. A. *Langmuir* **1996**, *12*, 145−153.
(2) Toney, M. F.; Fain, S. C., Jr. *Phys. Rev. B* **1984**, *36*, 1248−1258.
(3) Venkat, R. B.; Steele, W. A. *Langmuir* **1987**, *3*, 581−587.
(4) Hammonds, K. D.; McDonald, I. R.; Tildesley, D. J. *Mol. Phys.* **1990**, *70*, 175−195.
(5) Morishige, K. *Mol. Phys.* **1993**, *78*, 1203−1209.
(6) Mills, R. L.; Olinger, B.; Cromer, D. T.; Lesar, R. *J. Chem. Phys.* **1991**, *95*, 5392−5398.
(7) Terlain, A.; Larher, Y.; Angerand, F.; Parette, G.; Lauter, H.; Bassignana, I. C. *Mol. Phys.* **1986**, *58*, 799−813.
(8) Stranick, S. J.; Kamna, M. M.; Weiss, P. S. *Science* **1994**, *266*, 99−102.
(9) Trost, J.; Wintterlin, J.; Ertl, G. *Surf. Sci.* **1995**, *329*, L583−L587.
(10) Berner, S.; Brunner, M.; Ramoino, L.; Suzuki, H.; Guntherodt, H. J.; Jung, T. A. *Chem. Phys. Lett.* **2001**, *348*, 175−181.
(11) Yanagi, H.; Mukai, H.; Ikuta, K.; Shibutani, T.; Kamikado, T.; Yokoyama, S.; Mashiko, S. *Nano Lett.* **2002**, *2*, 601−604.
(12) McCarley, R. L.; Bard, A. J. *J. Phys. Chem.* **1992**, *96*, 7410−7416.
(13) Sawaguchi, T.; Yamada, T.; Okinaka, Y.; Itaya, K. *J. Phys. Chem.* **1995**, *99*, 14149−14155.
(14) Yamada, T.; Sekine, R.; Sawaguchi, T. *J. Chem. Phys.* **2000**, *113*, 1217−1227.
(15) Rodriguez, J. A.; Hrbek, J. *Acc. Chem. Res.* **1999**, *32*, 719−728.
(16) Chen, S. Y.; Smith, J. M.; McCoy, B. J. *J. Catal.* **1986**, *102*, 365−376.
(17) Hornstein, B. J.; Aiken, J. D.; Finke, R. G. *Inorg. Chem.* **2002**, *41*, 1625.
(18) Joshi, Y. P.; Tildesley, D. J.; Ayres, J. S.; Thomas, R. K. *Mol. Phys.* **1988**, *65*, 991.
(19) Dagg, I. R.; Anderson, A.; Yan, S.; Smith, W.; Joslin, C. G.; Read, L. A. A. *Can. J. Phys.* **1986**, *64*, 1475.
(20) Coriani, S.; Halkier, A.; Rizzo, A.; Ruud, K. *Chem. Phys. Lett.* **2000**, *326*, 269.
(21) Ferris, J. H.; Kushmerick, J. G.; Johnson, J. A.; Youngquist, M. G. Y.; Kessinger, R. B.; Kingsbury, H. F.; Weiss, P. S. *Rev. Sci. Instrum.* **1998**, *69*, 2691.
(22) Kardinal, I.; Netzer, F. P.; Ramsey, M. G. *Surf. Sci.* **1997**, *376*, 229.
(23) Barth, J. V.; Brune, H.; Ertl, G.; Behm, R. J. *Phys. Rev. B* **1990**, *42*, 9307.
(24) Stranick, S. J.; Kamna, M. M.; Weiss, P. S. *Surf. Sci.* **1995**, *338*, 41.
(25) Poirier, G. E. *Chem. Rev.* **1997**, *97*, 1117.
(26) Smolukowski, R. *Phys. Rev.* **1941**, *60*, 661.
(27) Sykes, E. C. H.; Han, P.; Weiss, P. S. *J. Phys. Chem. B* **2003**, *19*, 4500.
(28) Weiss, P. S.; Eigler, D. M. *Phys. Rev. Lett.* **1992**, *69*, 2240.
(29) Roder, H.; Hahn, E.; Brune, H.; Bucher, J. P.; Kern, K. *Nature* **1993**, *366*, 141.